Robust State Estimation for an Electricity-Gas-Heat Integrated Energy System Considering Dynamic Characteristics

Jianshu Yu, Dechang Yang, Jinye Cao, Payman Dehghanian, and Nikita Tomin

***Abstract*—The data for an energy management system (EMS) in an integrated energy system (IES) is obtained through state estimation. This is then the basis for optimal scheduling, protection and control. At present, the dynamic models of gas and heat networks are rarely considered in such state estimation, and the method lacks robustness. This paper develops dynamic state estimation models for gas and heat networks, and proposes a unified method for the electricity-gas-heat network, one which takes into account robustness while ensuring accuracy. First, the state transition equations in matrix form are formulated according to finite difference models considering the dynamic characteristics of the gas and heat networks. Then, combined with a quasi-steady state model of the electric power system, a unified state estimation method and multi-time-scale measurement strategy in the Kalman filter framework are proposed. In addition, the prediction accuracies of the electric power and gas systems are improved through adaptive adjustment. The kernel density estimation method is used to adjust the measurement weights and filter out bad data to ensure robust state estimation. Finally, simulation results show that the proposed method not only can improve the estimation accuracy by improving prediction accuracy, but also is robust to various types of bad data.**

***Index Terms*—Integrated energy system, electricity-gas-heat system, dynamic state estimation, robust state estimation, Kalman filter, nonparametric estimation.**

NOMENCLATURE

A. Indices

e	electrical power system
g	gas system
h	heat system
t	time index
i、j	node number of pipeline
F	front of pipeline
E	end of pipeline
$k(.)$	the set of pipelines whose front node is k
$(.)k$	the set of pipelines whose end node is k
x	location of the differential pipeline

B. General Parameters and Variables

A	cross-sectional area (m^2)
d	inner diameter (m)
l	pipe length (m)
P	gas pressure (Pa)
λ	friction coefficient
c	sound speed (m/s)
M	mass flow rate (kg/s)
ω	gas flow velocity (m/s)
R	gas constant

C. Heat System

m_{in}	mass flow rate within a pipe coming into the node (kg/s)
m_{out}	mass flow rate within a pipe leaving into the node (kg/s)
m_{q}	mass flow rate into the load (kg/s)
Φ_{h}	heat power
C_{p}	specific heat capacity of water
T_{s}	supply temperature (℃)
T_{o}	outlet temperature (℃)
T_{in}	water temperature within a pipe coming into the node (℃)
T_{out}	water temperature within a pipe leaving into the node (℃)
Z	measurement
X	state variable
L	load
L_{t}	typical daily load

D. Gas System

ρ_{g}	natural gas density (kg/m^3)
$\bar{\omega}$	average gas flow velocity (m/s)
ρ_{α}	gas density at the horizontal plane and at the plane with the inclination α

Received: February 27, 2023
Accepted: August 10, 2023
Published Online: Janauary 1, 2024
Dechang Yang (corresponding author) is with the College of Information and Electrical Engineering, China Agricultural University, Beijing 100084, China (e-mail: yangdechang@cau.edu.cn)
DOI: 10.23919/PCMP.2023.000142

z gas compressibility factor
ρ_w water density
T_g ambient temperature
k heat transfer coefficient

E. Coupling Element

CHP combine heat and power
Φ_{CHP} heat power of CHP
P_{CHP} electrical power of CHP
F_{in} consumption of natural gas
η_e electricity and gas conversion factor

I. Introduction

The fossil energy crisis and environmental pollution have accelerated the changes in energy structure, and key technologies related to energy coupling have been developed rapidly [1]–[2]. Consequently, how to improve energy utilization efficiency and promote the deep coupling among different energy sources has become an urgent problem [3]. To address the problem, the concept of the energy Internet has aroused widespread interest in researchers [4]–[5]. In the energy Internet, in addition to electricity, natural gas and heat/cold energy also play vital roles in energy supply. Therefore, an integrated energy system (IES) coupled with multi-energy flow is one of the main areas of research in the energy Internet. Compared with traditional single-type energy supply, IES-based multi-energy flow has higher conversion efficiency. However, because of the deep integration of energy and information flows, there exist many uncertainties in the system. Thus, the traditional energy management system (EMS) cannot meet the needs of an IES, and it is necessary to upgrade for multi-energy flow [6]. State estimation, as the perception part of the EMS, provides data for the energy flow calculation, protection and control, and optimization of the system [7]–[8]. Therefore, it is significant to study state estimation methods for IES.

At present, research on state estimation based on multi-energy flow model mainly consists of two aspects: static state estimation based on the steady-state model, and dynamic state estimation considering the dynamic characteristics of the gas and heat networks.

For static state estimation, a combined electricity-heat state estimation model is proposed in [9]. This increases measurement redundancy through coupling constraints. Compared with only a single energy flow network, it shows a better estimation result. On the basis of [9], the electricity-gas network is proposed for the energy Internet in [10]. The study shows that the electric-gas coupling is weak, which cannot improve the redundancy of measurement, though it is helpful for bad data identification at the boundary. The above two models use the traditional weighted least squares (WLS) method, which belongs to non-convex optimization and has difficulty in choosing the initial value. Combining the above gas and heat networks, a distributed state estimation algorithm based on the alternating direction multiplier method (ADMM) is proposed for three types of energy networks [11]. Here there is transformation of the problem, using the bilinear method, into a three-stage problem to avoid non-convex optimization. The bilinear method has also been applied to state estimation based on the weighted least absolute value (WLAV) method with an electricity-gas network in [12], electricity-heat network in [13], [14], and electricity-gas-heat network in [15]. The method adds robustness to the estimation results.

There are still two problems in static state estimation. The first is that when the load changes, only the steady-state results can be calculated through the multi-energy flow calculation, while the dynamic process at each moment cannot be reflected. However, the states of the gas and heat networks change slowly, while the load has changed before they reach a steady state. Thus, they are in a dynamic state most of the time, and the measured data cannot be used in the steady-state model. Second, there are significantly different dynamic processes among different energy flows, i.e., the state response in the power system is the fastest, followed by the natural gas system, while the heating system is the slowest. Compared with the state estimation for multi-energy networks at the same measurement frequency, the design for multi-time scale measurement is reasonable. Therefore, it is more meaningful to study the dynamic models that conform to their operating characteristics.

For integrated modeling of the electricity-gas-heat network, the time to steady-state is usually from a few minutes to a day, and the dynamic characteristics in an electric power system are much faster than those in the gas and heating systems. These last two can be regarded as quasi-steady state. The gas and heat networks need to consider the dynamic process [16], and the system state is calculated by the dynamic equation. At present, research on dynamic models is mainly on the following:

1) Finite difference model. The dynamic process of the gas and heat networks is usually described by a set of partial differential equations, which are solved by the finite difference method. In [17], the Euler difference scheme is used to solve the partial differential equations of natural gas, and then a robust scheduling model for the electricity-gas network is established. The more accurate Wendroff difference scheme is introduced in [18], [19], and a real-time optimal operation strategy of the electricity-gas combined system is proposed. The electricity-gas combined system proposed in [18], [19] is used in IES state estimation by [20], and an electricity-gas coupling network state estimation under the Kalman filtering framework is proposed. A distributed real-time state estimation method for electricity-heat systems is proposed in [21], where the Wendroff dif-

ference scheme is used to solve the partial differential equations of the heat network, and finally, a cubature Kalman filter (CKF) is used to calculate the system state. In [22], considering the various resistances in transmission, a more refined model for electric-heat energy flow calculation is proposed.

2) Pipeline storage model. Since gas can be compressed, the pipeline in the gas network is regarded as an energy storage element [23]. Transmission delay is considered in the heat network, and the water in the pipeline can be regarded as stored heat energy [24]. In [25], a time-delay model of the heat network is applied to the state estimation for a combined heat and power system, and a hybrid method with a two-stage iterative algorithm is proposed. This has good performance even when the measurement number is limited. Although the model is easy to understand and is widely used for optimal scheduling of electricity-gas and electricity-heat combined systems, the relationship between the state variables in the model is not clear, and the state transition equation is not easy to derive.

3) Energy circuit theory. In [26], [27] and [28], [29], the pipelines in gas and heat networks are respectively compared with the components in the electricity network, and the 'gas circuit' and 'heating circuit' are proposed and analyzed from the perspective of the electrical circuit. Finally, a unified energy circuit model is established by the complex frequency domain. The perfect unification in the mathematical form helps us to study other physical models with the theory of the electric power system. This simplifies the model and makes the characteristics of different energy networks more intuitive. However, the essentially different energy properties between gas, heat, and electricity networks make it impossible to establish a completely unified model without any assumptions, and the approximate modeling may lead to loss of accuracy.

Research on the dynamic state estimation for IES is mostly based on the analysis of two kinds of energy networks, and there is limited unified modeling for the three kinds of energy networks. There is no unified solution framework for the system coupled with those three networks. At present, the dynamic model or quasi-steady-state model of a power system is usually converted into a time series model [16]. A priori estimation is performed through the state transition equation, while on the basis of the prior estimation results, an a posteriori estimation is then performed considering the measurement. The commonly used algorithm is the Kalman filter and its improved algorithm. Among the above three models, the finite difference model is the most suitable for existing power system state estimation methods, through which the mathematical relationship of the system state in time and space can be clearly described. Therefore, based on the finite difference model, this paper deduces the state transition equations of the heat and gas networks in the form of a matrix, so that the existing electric power system state estimation methods can be directly applied to the thermal and natural gas systems. In addition, a unified solution framework for IES state estimation is established.

The deep coupling of multiple energy systems will increase the influence of bad data, while the IES dynamic state estimation based on the Kalman filter is not sufficiently robust. If the bad data identification link based on the largest normalized residual is added, it is necessary to continuously remove the bad data and re-estimate. This will lead to low computational efficiency. For static IES state estimation, there have been many studies on robustness [12]–[15], but they cannot be applied to Kalman filtering.

In view of the above problems, combined with the existing dynamic models and state estimation methods, this paper proposes a robust state estimation method for electricity-gas-heat networks. The main contributions are:

1) The dynamic characteristics of the electricity, gas, and heat networks are analyzed, and the state transition equations in matrix form are established by the finite difference method. A unified state estimation method is proposed.

2) The prediction steps for the electricity and gas networks are improved, and the prediction accuracy is improved through their adaptive adjustment.

3) From the speed of dynamic characteristics in different networks, a multi-time scale measurement strategy is proposed, and the influence of different measurement time scales on the state estimation is discussed and analyzed.

4) Non-parametric estimation is carried out through the kernel density method to adjust the measurement weight adaptively so that the state estimation still has robustness without bad data identification.

II. IES Model Considering Dynamic Characteristics

The modeling of an IES includes the electric, natural gas, and heating systems. Since the electricity network is regarded as a quasi-steady state, the dynamic process is ignored. The AC steady-state mode is usually used to describe the electricity network in an IES [30], and no detailed description is provided here.

A. Dynamic Energy Flow of Gas Network

1) Dynamic Equations of Gas Pipeline

Ignoring the temperature change, the gas flow in the pipeline is usually described by the following three equations [18]: the momentum equation in (1), the material-balance equation in (2), and the state equation in (3).

$$\frac{\partial(\rho_g \omega)}{\partial t} + \frac{\partial(\rho_g \omega^2)}{\partial x} + \frac{\partial p}{\partial x} + g(\rho_g - \rho_\alpha)\sin\alpha + \frac{\lambda}{d}\frac{\omega^2}{2}\rho_g = 0 \tag{1}$$

$$\frac{\partial \rho}{\partial t}+\frac{\partial \rho \omega}{\partial x}=0 \tag{2}$$

$$p/\rho = zRT = c^2 \tag{3}$$

The momentum and material relationships in natural gas are described by (1) and (2), respectively. Assuming both temperature T and gas compressibility factor z are constant, $zRT=c^2$ is used to simplify the description of the relationship between pressure and density in (3).

Equations (1) and (2) are very complex and difficult to solve directly by the finite difference method. Referring to [18], they can be appropriately simplified under the following assumptions:

1) The altitude does not change along the pipes, and then $\alpha = 0$.

2) Neglect the second term (convection term) in (1), which is meaningful only when the gas velocity is close to the speed of sound, while the pipeline velocity is generally 20–40 m/s.

3) The quadratic term ω^2 in (1) is represented by the average flow rate.

4) The flow of natural gas in the pipeline is expressed by mass flow rate M (kg/s), while M is calculated by:

$$M = \rho \omega A \tag{4}$$

Under the above assumptions, the momentum equation (1) and material-balance equation (2) are transformed to:

$$\frac{\partial M}{A\partial t}+c^2\frac{\partial \rho}{\partial x}+\frac{\lambda \bar{\omega}}{2dA}M=0 \tag{5}$$

$$\frac{\partial \rho}{\partial t}+\frac{\partial M}{A\partial x}=0 \tag{6}$$

2) Linearization of Dynamic Equations in Gas Network

The Lax-Wendroff finite difference method is used to solve partial differential equations, as:

$$\begin{cases}\dfrac{\partial X}{\partial t}=\dfrac{1}{2}\left(\dfrac{X_{i+1}^{t+1}-X_{i+1}^{t}}{\Delta t}+\dfrac{X_{i}^{t+1}-X_{i}^{t}}{\Delta t}\right)\\ \dfrac{\partial X}{\partial x}=\dfrac{1}{2}\left(\dfrac{X_{i+1}^{t+1}-X_{i}^{t+1}}{\Delta x}+\dfrac{X_{i+1}^{t}-X_{i}^{t}}{\Delta x}\right)\end{cases} \tag{7}$$

The differential pipeline is shown by Fig. 1. Equation (7) is replaced by (5) and (6), and written as a matrix form [20]:

$$\begin{bmatrix}-\boldsymbol{A}_4^{ij} & \boldsymbol{A}_4^{ij} & \boldsymbol{A}_3^{ij}+\boldsymbol{A}_5^{ij} & \boldsymbol{A}_3^{ij}+\boldsymbol{A}_5^{ij}\\ \boldsymbol{A}_1 & \boldsymbol{A}_1 & -\boldsymbol{A}_2^{ij} & \boldsymbol{A}_2^{ij}\end{bmatrix}\begin{bmatrix}\rho_i^{t+1}\\ \rho_j^{t+1}\\ M_i^{t+1}\\ M_j^{t+1}\end{bmatrix}=$$
$$\begin{bmatrix}\boldsymbol{A}_4^{ij} & -\boldsymbol{A}_4^{ij} & \boldsymbol{A}_3^{ij}-\boldsymbol{A}_5^{ij} & \boldsymbol{A}_3^{ij}+\boldsymbol{A}_5^{ij}\\ \boldsymbol{A}_1 & \boldsymbol{A}_1 & \boldsymbol{A}_2^{ij} & -\boldsymbol{A}_2^{ij}\end{bmatrix}\begin{bmatrix}\rho_i^{t}\\ \rho_j^{t}\\ M_i^{t}\\ M_j^{t}\end{bmatrix} \tag{8}$$

$$\boldsymbol{A}_1=1;\boldsymbol{A}_2^{ij}=\frac{\Delta t}{\Delta x_{ij}\boldsymbol{A}_{ij}};\boldsymbol{A}_3^{ij}=\frac{1}{\boldsymbol{A}_{ij}};$$
$$\boldsymbol{A}_4^{ij}=\frac{c^2\Delta t}{\Delta x_{ij}};\boldsymbol{A}_5^{ij}=\frac{\lambda_{ij}\bar{\omega}_{ij}^{t}\Delta t}{4d_{ij}\boldsymbol{A}_{ij}} \tag{9}$$

A pipeline can be regarded as several pipelines connected in series after finite difference, and the length is the difference space step Δx, as shown in Fig. 1. There are 4 state variables for each pipeline, i.e., M_i and M_j are the mass flow rates at the front and end of the pipeline, respectively; while ρ_i and ρ_j represent the respective gas densities at the front and end of the pipeline.

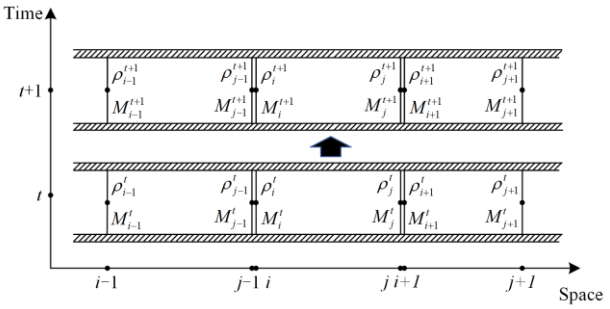

Fig. 1. Pipeline in the gas network after finite difference.

3) Boundary Conditions

It can be seen from (8) that the state transition matrix with full rank cannot be established according to the linearized dynamic equation, and the boundary conditions need to be added to make the solution of the state transition equations unique. The boundary conditions are shown in Fig. 2 and given as:

$$p_i^t = p_{\text{source}} \tag{10}$$

$$p_{F(i+1)(j+1)}^t = p_{Eij}^t \tag{11}$$

$$M_{F(i+1)(j+1)}^t = M_{Eij}^t \tag{12}$$

$$\sum_{i\in k(.)} M_{Fki}^t = \sum_{j\in(.)k} M_{Ejk}^t - M_{k,\text{load}}^t \tag{13}$$

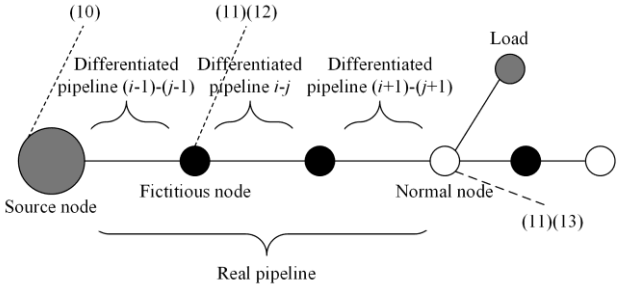

Fig. 2. Boundary conditions for nodes and pipes.

The pressure of the gas source node is constant, and the mass flow rate satisfies the dynamic equation. This is used to balance the load change, so (10) needs to be satisfied. The nodes used to connect the differential pipelines are fictitious, and the values of pressure and

mass flow rates at those nodes are unique, so they need to satisfy (11) and (12). At the real nodes, the pressure value is considered to be unique, while the mass flow rate is divided into the flow before confluence (at the end of the pipe) and the flow after confluence (at the front of the pipe), and need to satisfy the flow balance equation (13).

Finally, combining (8)–(13), the state transition equations in matrix form can be established by:

$$\begin{aligned}&\begin{bmatrix}\boldsymbol{J}_1\\ \boldsymbol{J}_3\end{bmatrix}^{\mathrm{T}}\boldsymbol{X}_g^{t+1}=\begin{bmatrix}\boldsymbol{J}_2\\ 0\end{bmatrix}^{\mathrm{T}}\boldsymbol{X}_g^{t}+\boldsymbol{C}_g\\ &\boldsymbol{X}_g^{t}=\left[\rho_{F12}^{t},\rho_{E12}^{t},M_{F12}^{t},M_{E12}^{t},\cdots\right]^{\mathrm{T}}\end{aligned}\tag{14}$$

where $\boldsymbol{J}_1$ and $\boldsymbol{J}_2$ are the coefficient matrices of the equations in (8); while $\boldsymbol{J}_3$ and $\boldsymbol{C}_g$ are the coefficient matrix and constant vector of the equations respectively constructed by (10)–(13).

B. Dynamic Energy Flow of Heat Network

A quantity control method is used to regulate the power of the heat network. In this approach, the primary means of meeting power demand is by adjusting the water flow rate through heat exchangers, while keeping the supply water temperature and return water temperature constant. The heat network model usually consists of a thermal model and a hydraulic model. The hydraulic model is used to describe the distribution of flow, and the thermal model is used to describe the flow of power. The mass flow rate can reach a steady state within a few seconds, but the transfer of heat energy may be delayed for tens of minutes. Therefore, only the temperature in the heat network is estimated, and the change of water velocity is regarded as a quasi-steady state.

1) Hydraulic Model

The flow continuity equation needs to be satisfied in the hydraulic model, i.e., the total flow into the node equals the total flow out of the node plus the flow into the load, i.e.:

$$\sum m_{\mathrm{in}}=\sum m_{\mathrm{out}}+m_{\mathrm{q}}\tag{15}$$

2) Node Thermal Power Model

The thermal power of the heat source and load node is expressed by:

$$\Phi_{\mathrm{h}}=C_{\mathrm{p}}m_{\mathrm{q}}(T_{\mathrm{s}}-T_{\mathrm{o}})\tag{16}$$

3) Node Temperature Mixture Model

After the water is mixed at the node, the temperature will change. According to the law of conservation of energy, the power flowing into the node equals the power flowing out of the node, i.e.

$$(\sum m_{\mathrm{out}})T_{\mathrm{out}}=\sum m_{\mathrm{in}}T_{\mathrm{in}}\tag{17}$$

4) Dynamic Heat Transfer Model in the Pipeline

The heat of the heat network is transferred through the flow of water. There is heat loss in the process, so the temperature will change. The dynamic characteristics can be described by the partial differential equation, as:

$$\rho_{\mathrm{w}}C_{\mathrm{p}}A\frac{\partial T_x^t}{\partial t}+mC_{\mathrm{p}}\frac{\partial T_x^t}{\partial x}=k(T_{\mathrm{g}}-T_x^t)\tag{18}$$

When it reaches a steady state, the partial differential of temperature with respect to time is negligible, and thus (18) degenerates into a steady-state expression, as:

$$T_{\mathrm{end}}=(T_{\mathrm{start}}-T_{\mathrm{g}})e^{-\frac{kL}{C_{\mathrm{p}}m}}+T_{\mathrm{g}}\tag{19}$$

To solve (18), a first-order Taylor expansion is used to express T_x^t:

$$\begin{aligned}\frac{\partial T_x^t}{\partial x}&=\frac{T_x^t-T_{x-\Delta x}^t}{\Delta x}\\ \frac{\partial T_x^t}{\partial t}&=\frac{T_x^t-T_x^{t-\Delta t}}{\Delta t}\end{aligned}\tag{20}$$

Substituting (20) into (18), the state transition equation for temperature is solved by:

$$\begin{aligned}&T_{x,t}-AT_{x-\Delta x}^t=BT_x^{t-\Delta t}+C\\ &A=\frac{mC_{\mathrm{p}}\Delta t}{\rho C_{\mathrm{p}}A\Delta x+mC_{\mathrm{p}}\Delta t+k\Delta t\Delta x}\\ &B=\frac{\rho C_{\mathrm{p}}A\Delta x}{\rho C_{\mathrm{p}}A\Delta x+mC_{\mathrm{p}}\Delta t+k\Delta t\Delta x}\\ &C=\frac{kT_{\mathrm{g}}\Delta t\Delta x}{\rho C_{\mathrm{p}}A\Delta x+mC_{\mathrm{p}}\Delta t+k\Delta t\Delta x}\end{aligned}\tag{21}$$

Compared with the gas network, the state variable of the heat network is only temperature, and the dynamic characteristics are simpler. The differential pipelines are shown in Fig. 3. In the heat network, only the temperatures at the fictitious nodes or real nodes are considered as state variables, and the front or end of the pipeline is not distinguished.

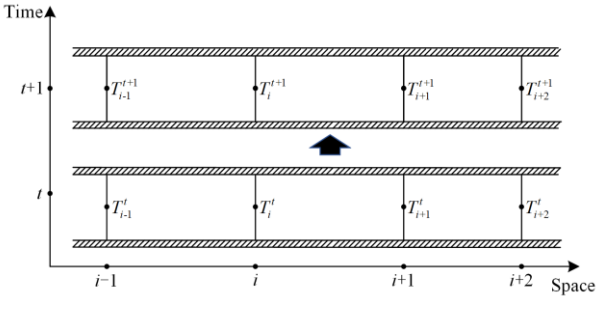

Fig. 3. Pipeline in the heat network after finite difference.

5) Boundary Conditions

The temperature constraint at the inlet of each real pipeline should be considered. The pipes connecting the heat source need to meet (22), while the pipes connecting other pipes need to meet (23).

$$T_{0,t}=T_{\mathrm{source}}\tag{22}$$

$$T_{\text{out},t}=\frac{\sum\left(m_{\text{in}}T_{\text{in}}\right)}{\sum m_{\text{out}}}=\sum\left(\frac{m_{\text{in}}}{\sum m_{\text{out}}}T_{\text{in}}\right) \tag{23}$$

The source temperature is constant, so the first pipe needs to satisfy (22). For other pipes, the water flowing into the pipe is mixed water, and (23) can be obtained from (17).

Considering the constraints (22) and rewriting (21), the state transition equation in matrix form of the first pipeline can be represented by:

$$\begin{aligned}&\boldsymbol{J}_{A_0}\boldsymbol{T}_{h_0}^{t+1}=\boldsymbol{J}_{B_0}\boldsymbol{T}_{h_0}^{t}+\boldsymbol{J}_{C_0}\\&\boldsymbol{T}_{h_0}^{t}=\left[T_0^t,T_1^t,\ldots,T_n^t\right]^{\mathrm{T}}\end{aligned} \tag{24}$$

$$\begin{aligned}&\boldsymbol{J}_{A_0}=\begin{bmatrix}1&&&&\\-A&1&&&\\&-A&1&&\\\cdots&\cdots&\cdots&\cdots&\cdots\\&&&-A&1\end{bmatrix},\\&\boldsymbol{J}_{B_0}=\begin{bmatrix}0&&&&\\&B&&&\\&&B&&\\\cdots&\cdots&\cdots&\cdots&\cdots\\&&&&B\end{bmatrix},\boldsymbol{J}_{C_0}=\begin{bmatrix}C_{\text{s}}\\C\end{bmatrix}\end{aligned} \tag{25}$$

where C_{s} is the source temperature.

The state transition matrices of all pipelines need to be combined to create the state equations for all variables. First, equations (26) and (27) are built according to (24) and (25).

$$\begin{aligned}&\boldsymbol{J}_A'\boldsymbol{X}_h^{t+1}=\boldsymbol{J}_B\boldsymbol{X}_h^{t}+\boldsymbol{J}_C\\&\boldsymbol{X}_h^{t}=\left[T_{h_0}^t,T_{h_1}^t,\ldots,T_{h_n}^t\right]^{\mathrm{T}}\end{aligned} \tag{26}$$

$$\begin{aligned}&\boldsymbol{J}_A'=\begin{bmatrix}\boldsymbol{J}_{A_0}&&&\\&J_{A_1}&&\\&&\ddots&\\&&&J_{A_n}\end{bmatrix},\\&\boldsymbol{J}_B=\begin{bmatrix}\boldsymbol{J}_{B_0}&&&\\&J_{B_1}&&\\&&\ddots&\\&&&J_{B_n}\end{bmatrix},\boldsymbol{J}_C=\begin{bmatrix}\boldsymbol{J}_{C_0}\\J_{C_1}\\\vdots\\J_{C_n}\end{bmatrix}\end{aligned} \tag{27}$$

In $\boldsymbol{J}_{C_i},i=0,1,\ldots,n$, $C_{\text{s}}=0$ for nodes not connected to the source.

Equation (23) reflects the connection between different real pipelines and can be written into the state transition matrix only when the state equations of all pipelines are combined. Therefore, the coefficients in (23) can be written into J_A' to obtain $\boldsymbol{J}_A$, and the final state transition matrix can be expressed by:

$$\boldsymbol{J}_A\boldsymbol{X}_h^{t+1}=\boldsymbol{J}_B\boldsymbol{X}_h^{t}+\boldsymbol{J}_C \tag{28}$$

In the state transition equation, the mass flow rate is an unknown variable. Since it is regarded as a quasi-steady state in the heat network, the steady-state value is used as an approximation to simplify the calculation. According to (15)–(17), (19) and the node loads, the nonlinear equations for the steady-state model can be established and then solved by the Newton-Raphson method. For the specific solution process, please refer to [31].

C. Coupling Element Model

In this paper, the combined heat and power (CHP) unit including the micro-combustion turbine and the electric boiler are used as the main coupling components. The energy relation is expressed by:

$$c_m=\frac{\Phi_{\text{CHP}}}{P_{\text{CHP}}} \tag{29}$$

$$F_{\text{in}}=\frac{P_{\text{CHP}}}{\eta_{\text{e}}} \tag{30}$$

There are two operating modes in CHP, i.e., following the thermal load (FTL), and following the electric load (FEL). Only the FTL mode is considered in this paper, so the CHP unit is used as the balance node of the heat network, and the electrical power output in CHP varies with thermal power output.

III. IES State Estimation Based on Kalman Filter

A. Measurement and State Variables in IES

$$\begin{aligned}&X=\begin{cases}X_e=[u_i,\theta_i]\\X_g=[p_i,M_{Fij},M_{Eij}]\\X_h=[T_{\text{s}},T_{\text{r}}]\end{cases}\\&Y=\begin{cases}Y_e=[u_i,\theta_i,P_i,Q_i,P_{ij},Q_{ij}]\\Y_g=[p_i,M_{Fij},M_{Eij}]\\Y_h=[T_{\text{s}},T_{\text{r}}]\end{cases}\end{aligned} \tag{31}$$

The state variables in the electric power system are voltage amplitude and phase angle, and the measurements include voltage amplitude, phase angle, node power, and branch power. The state variables and measurements in the gas network are the pressures at the real nodes and the mass flow rates at the front and end of the pipeline. The state variables and measurements in the heat network are the supply and return temperatures of the nodes. The return and supply pipelines are symmetrical, so the calculation method of the return water temperature is the same as that of the supply water.

B. Measurement Equation and State Transition Equation

The relationship between measurements and state variables in the electric power system is non-linear, and

the equations cannot be solved directly by the Kalman filter. Thus, it needs first to be linearized. Based on the method of extended Kalman filtering, there are:

$$\begin{aligned} Z_e^t &= H_e^t X_e^t + R_e^t \\ H_e^t &= \frac{\partial H(X_e^t)}{\partial X_e^t} \end{aligned} \tag{32}$$

where $H(X_e^t)$ is a nonlinear measurement function, and only the first-order Taylor expansion is performed while high-order terms are ignored. R_e^t is the measurement noise.

In the gas and heat networks, the measurements are the same as the state variables, and the state transition equations are expressed by:

$$\begin{aligned} Z_g^t &= X_g^t + R_g^t \\ Z_h^t &= X_h^t + R_h^t \end{aligned} \tag{33}$$

A quasi-steady state model is used in the electric power system, and Holt's linear exponential smoothing method is usually used to establish the state transition equation, as:

$$\begin{cases} \tilde{X}_{t\mid t-1} = a_{t-1} + b_{t-1} \\ a_{t-1} = \alpha \hat{X}_{t-1\mid t-1} + (1-\alpha)\tilde{X}_{t-1\mid t-2} \\ b_{t-1} = \beta\left(a_{t-1} - a_{t-2}\right) + (1-\beta) b_{t-2} \end{cases} \tag{34}$$

where $\tilde{x}_{t\mid t-1}$ represents the predicted value of the state variable at time t to time t-1; and $\hat{X}_{t-1\mid t-1}$ is the estimated value at time t-1; α and β are smoothing coefficients in the range of [0,1].

The gas and heat networks have been linearized by finite difference, and the state transition equations in matrix form are constructed in (14) and (28). These can be solved directly by the Kalman filter algorithm.

C. State Estimation by Kalman Filter

1) Prediction Step

The state prediction value can be calculated by the state transition equation (35), and the covariance matrix before the measurement update can be calculated by (36).

$$\begin{aligned} &\tilde{\boldsymbol{X}}^{t+1} = f(\tilde{\boldsymbol{X}}^t) \\ &\begin{cases} \tilde{\boldsymbol{X}}_e^{t+1} = f_{\text{holt}}(\tilde{\boldsymbol{X}}_e^t) \\ \tilde{\boldsymbol{X}}_g^{t+1} = \left(\begin{bmatrix} \boldsymbol{J}_1 \\ \boldsymbol{J}_3 \end{bmatrix}^{\mathrm{T}}\right)^{-1} \begin{bmatrix} \boldsymbol{J}_2 \\ 0 \end{bmatrix}^{\mathrm{T}} \tilde{X}_g^t + \left(\begin{bmatrix} \boldsymbol{J}_1 \\ \boldsymbol{J}_3 \end{bmatrix}^{\mathrm{T}}\right)^{-1} \boldsymbol{C}_g \\ \tilde{\boldsymbol{X}}_h^{t+1} = \boldsymbol{J}_A^{-1} \boldsymbol{J}_B \tilde{X}_h^t + \boldsymbol{J}_A^{-1} C_h \end{cases} \end{aligned} \tag{35}$$

$$\begin{aligned} &\tilde{\boldsymbol{P}}^{t+1} = \boldsymbol{F} P^t F^{\mathrm{T}} + Q \\ &\begin{cases} \boldsymbol{F}_e = \alpha I \\ \boldsymbol{F}_g = \left(\begin{bmatrix} \boldsymbol{J}_1 \\ \boldsymbol{J}_3 \end{bmatrix}^{\mathrm{T}}\right)^{-1} \begin{bmatrix} \boldsymbol{J}_2 \\ 0 \end{bmatrix}^{\mathrm{T}} \\ \boldsymbol{F}_h = \boldsymbol{J}_A^{-1} \boldsymbol{J}_B \end{cases} \end{aligned} \tag{36}$$

where Q is the process noise, which is assumed to follow a Gaussian distribution.

2) Correction to the Prediction Step

By Holt's method, the current value is calculated by a weighted average of the most recent past values, with weights decreasing over time. System states in the short-term can be quickly predicted by this method, but when large disturbances in the load occur, the accuracy will be significantly affected. This problem can be improved by limiting the weights of the predicted values, as [32]:

$$\begin{aligned} W_t^{\text{new}}(j) &= W_t^{\text{new}}(j) \exp(-\left|\hat{x}_{t-1}(j) - \hat{x}_{t-2}(j)\right|^2) \\ Q(j,j) &= \frac{1}{W_t^{\text{new}}(j)} \end{aligned} \tag{37}$$

It can be seen from (37) that when the states at adjacent moments are not much different, it means that the load change is not large at this moment, and $\exp(-\left|\hat{x}_{t-1}(j) - \hat{x}_{t-2}(j)\right|^2)$ is close to 1, so that the process noise is almost unchanged. When the difference between them is large, it means that the load change is also large, and the reliability of Holt's method becomes lower, so the process noise also increases.

For the gas and heat networks, the state transition equations are derived from physical models, so the prediction accuracy is high. However, when the load fluctuates, the state variables in the gas network will oscillate and attenuate. The amplitude increases as the difference time step increases, and the accuracy of the prediction decreases. Therefore, the prediction accuracy is improved by reducing the change rate of the predicted value, as:

$$\tilde{X}_g^{t+1} = \hat{X}_g^{t-1} + (\hat{X}_g^{t+1} - \hat{X}_g^{t-1}) \exp(-\mu \left| \hat{X}_g^{t+1} - \hat{X}_g^{t-1} \right|^2) \tag{38}$$

As seen from (38), when the predicted value at this moment is not much different from the estimated value at the previous moment, the predicted value will hardly change. Conversely, if it fluctuates greatly, the second term in (38) will reduce its change step size. μ is an adjustable parameter with a small value to prevent failure of the predicted value.

Because the heat network model is relatively simple, the prediction accuracy is high, and larger fluctuations rarely occur, so it is not necessary to modify the prediction step.

3) Update Step

The Kalman gains of the three networks can be calculated by:

$$\boldsymbol{K} = \frac{\tilde{\boldsymbol{P}}^{t+1} \boldsymbol{H}^{\mathrm{T}}}{\boldsymbol{H} \tilde{\boldsymbol{P}}^{t+1} \boldsymbol{H}^{\mathrm{T}} + \boldsymbol{R}} \tag{39}$$

where $\boldsymbol{H}$ is the measurement matrix. The measurement matrix of the electric power system has been linearized by (32), and the measurement matrices of the gas and heat networks are the identity matrices:

$$\hat{\boldsymbol{X}}^{t+1}=\hat{\boldsymbol{X}}^{t}+\boldsymbol{K}(\boldsymbol{Z}-\boldsymbol{H}(\hat{\boldsymbol{X}})) \tag{40}$$

The measurement function of the electric power system in (40) does not need to be linearized, so the predicted values are directly substituted. Finally, the state estimation at time t is completed once the updated covariance matrix is calculated by:

$$\boldsymbol{P}^{t+1}=\left(\boldsymbol{I}-\boldsymbol{K}\boldsymbol{H}\right)\tilde{\boldsymbol{P}}^{t+1} \tag{41}$$

4) Multi-time Scale Measurement Strategy

Because of the great differences in physical properties and system scale of each subsystem, they have significantly different dynamic characteristics, as shown in Fig. 4.

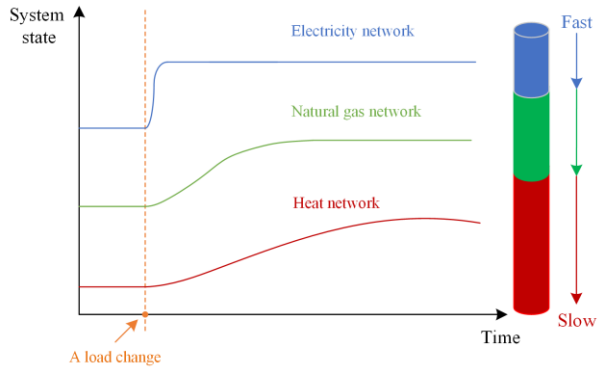

Fig. 4. The dynamic process of energy networks with different physical properties.

The dynamic response speed of the electricity, gas and heat networks decreases in turn. The state variables in a network with a fast response speed are difficult to predict, while a faster measurement frequency is required to ensure prediction accuracy. Therefore, a multi-time scale measurement strategy is proposed in this paper, as shown in Fig.5.

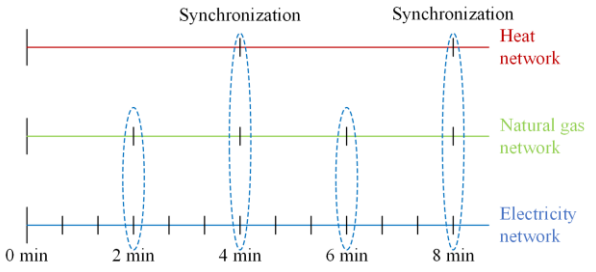

Fig. 5. Multi-time scale measurement strategy.

Assuming that the sampling times of the electricity, gas and heat networks are 1 min, 2 min and 4 min respectively, then the electricity and gas networks can be synchronized every 2 min, and the three electricity-gas-heat networks can be synchronized every 4 min. The method not only satisfies the different dynamic characteristics of each sub-network but also ensures the coupling constraints between each network. Through the measurement strategy, different dynamic characteristics of each sub-network are satisfied, and the coupling constraints between each network are ensured.

IV. Robust State Estimation for IES Based on Nonparametric Estimation

A. Proposition of Kernel Density Estimation Method

In the previous descriptions, a unified state estimation model in the Kalman filter framework is established by linearizing the measurement function and the state transition equation. However, the state estimation method is not robust to bad data. Identifying bad data by maximizing normalized residuals may lead to the elimination of valid data, and requires re-estimation, which is inefficient. The measurement is used in the update step of the Kalman filter, so if the measurement can be directly judged (i.e., whether it is bad data or not) based on the result of the prediction step, the efficiency can be greatly improved. The most direct way is to set a threshold for s, with $s=\left|Z-H(\tilde{x}_k)\right|$ being the difference of the measured values and predicted values. If the value is too large, it considers that it is bad data. Even if there is an error in the predicted value, it has a high probability of appearing near the true value. However, bad data may occur in the measurement because of data transmission, measurement equipment failure, etc. When the difference between the measurement and the prediction is large, it is more likely that the measurement has bad data. However, the accuracy of the predicted value is not stable, and it is related to the change rate of the system state. When the state of the system changes rapidly, the prediction accuracy will also decrease. Therefore, it is not feasible to simply set a threshold which does not consider the prediction accuracy. In addition, only removing bad data by threshold will make the estimated results not smooth and lack stability because it may lead to misjudgment as the measurement redundancy is reduced.

In view of the above problems, to ensure the smoothness of the state estimation results and eliminate the influence of bad data, the measurement data are processed as follows:

1) Instead of removing bad data directly by threshold setting, the influence of bad data is weakened by changing the weight of measurement, which can prevent effective measurements from being rejected.

2) The weight of measurement is determined by $p(s)$, which is the probability density of s. Replacing the absolute value with the probability density of s is to eliminate the effect of prediction error. If the prediction accuracy is low for a certain period of time, it will lead

to large deviation values with large probability density.

The explicit expression of the probability distribution function cannot be directly calculated, but with the help of nonparametric estimation methods, it can be obtained from historical samples, avoiding the need to solve the probability distribution function. In nonparametric estimation, the kernel density estimation is a commonly used method.

Kernel density estimation (KDE), also known as Parzen window technique, is a nonparametric estimation method. It does not need to solve the parameters of the probability density function, but uses a superposition of a set of standard functions to represent the function.

The samples $s_i, i=1,\ldots n$ in the *d*-dimensional space obey some unknown distribution. Given the kernel function $K(s)$, the probability density of variable s can be obtained from the samples, shown as:

$$p(s)=\frac{1}{nh^d}\sum_{i=1}^{n}K\left(\frac{s-s_i}{h}\right) \tag{42}$$

where h is the window radius of the kernel function. This is set manually. The kernel function needs to ensure that the value of $K\left(\frac{s-s_i}{h}\right)$ decreases as the distance between the estimated point s and the sample s_i increases. $\frac{1}{nh^d}$ is used to ensure that the integration of $p(s)$ is 1, making it a valid probability density function.

The Gaussian kernel is used as the kernel function, as:

$$K(s)=(2\pi)^{-d/2}\exp\left(-\frac{1}{2}\|s\|^2\right) \tag{43}$$

B. Application of Kernel Density Estimation in IES Robust State Estimation

1) Kernel Density Estimation for Measurement Weights

With the help of kernel density estimation, the probability density on the measurement is calculated. The weights of the measurement data are adaptively adjusted to make the state estimation robust. Equation (38) can be rewritten as:

$$\hat{X}^{t+1}=\tilde{X}^{t}+K\left[W(Z-H(\tilde{X}))\right] \tag{44}$$

The weight value does not need to be a legal probability density function, so the weight can be represented by:

$$w=\frac{1}{n}\sum_{i=1}^{n}\exp\left(-\frac{1}{h}\left|s-s_i\right|^2\right) \tag{45}$$

Kernel density estimation is calculated based on historical samples, and the selection of samples is directly related to the validity of the calculation results. The most important factor affecting the prediction accuracy is the change rate of the system state. This is positively related to the load change rate. The load change is related to time and has a certain regularity and periodicity. Therefore, the historical data of the current time period can be used as samples for estimation.

2) Data Generation Based on Monte Carlo Method

Considering that the load may vary periodically with the season, based on a typical day of a season, minute-level data are generated by interpolation, and 90-day load data are generated by:

$$\begin{aligned} &L(1)\sim N(L_{\mathrm{t}}(1),\sigma^2)\\ &L(t)=L(t-1)+\lambda \end{aligned} \tag{46}$$

$$\begin{aligned} &\lambda\sim N(dL,(\eta dL)^2)\\ &dL=L_{\mathrm{t}}(t)-L_{\mathrm{t}}(t-1) \end{aligned} \tag{47}$$

where L_{t} and L represent the typical day load and the randomly generated load, respectively. σ is the standard deviation of the initial value. η is an adjustable parameter, and the larger the value, the greater the randomness of the load.

Equation (46) ensures the randomness of the initial value, and the data generated by (47) can ensure that the generated load not only has the variation characteristics of a typical daily load, but also can increase the load fluctuation by adjusting η. Finally, the generated loads are simulated and a historical database about s is established.

3) Data Sampling

To ensure calculation efficiency, not all samples are considered in each calculation, and N1 days can be randomly selected from the historical database. Considering that the load change rate is different in each time period, the accuracy of state prediction will also be affected. Therefore, N2 samples are sampled within one hour before and after the current estimated time. Finally, a total of N1×N2 samples are obtained for each measurement value.

C. Calculation Process

The calculation process is shown in Fig. 6 and is described below. First, the estimated system in the current time is determined according to the multi-time scale measurement strategy, and then the relevant parameters in the state transition matrix are updated and the state variables are predicted. Subsequently, the prediction values of the electricity and gas networks are corrected by (40) and (41). Finally, the historical data are sampled and the measurement weights are determined according to the kernel density estimation, and the predicted values are updated by (44).

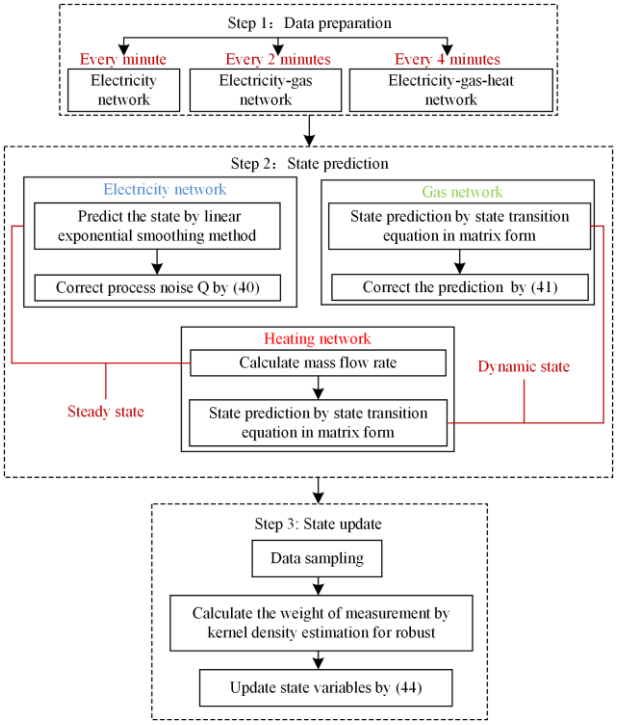

Fig. 6. Robust state estimation calculation process for IES.

V. Case Study

A. Case Description

The case study of an electricity-gas-heat IES is shown in Fig. 7. As seen, there are 7 load nodes and 3 generators in the electricity network. G1 is a gas turbine with a conversion efficiency of 1.8 (MW·s/kg), and G2 is the power grid, which is regarded as the slack node of the electric power system. The working mode of CHP is FTL and the output ratio of heat and electricity is 1.3. In the heat network, H8 is the heat source, which is supplied by CHP, and the source temperature is set to 100 °C. The other nodes are load nodes, the outlet water temperature is 50 °C, and the ambient temperature is set to 10 °C. There are 4 load nodes and one gas source in the natural gas network. The pressure of the gas source is set to 3×10^7 Pa. G2 and G5 provide natural gas for the gas turbine and CHP, respectively.

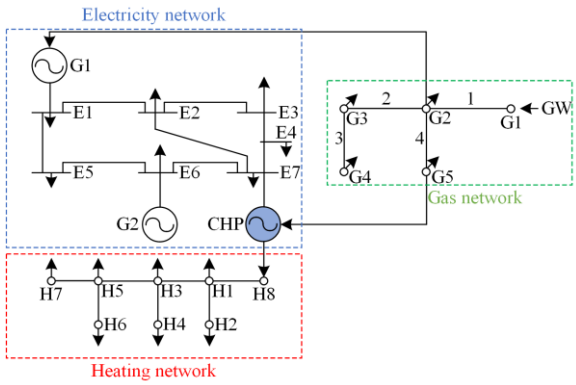

Fig. 7. Electricity-gas-heat coupling network topology.

The hourly load demands of electricity, heat, and natural gas in a day are shown in Fig. 8, and the load data at any time can be obtained by (46) and (47).

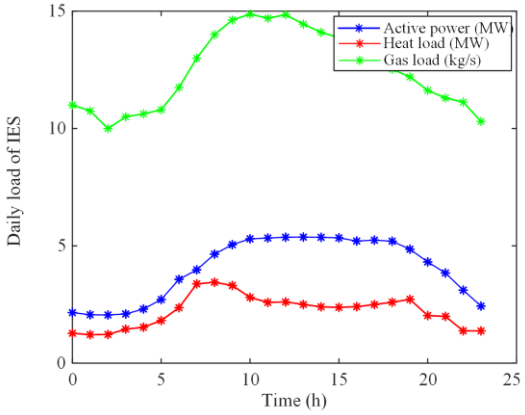

Fig. 8. Daily load demand of IES.

The load adjustment periods of the gas network and heat network are set to 10 min and 20 min respectively, while the sampling periods of the electricity network, gas network and heat network are 1 min, 2 min and 4 min respectively.

According to the load of the day, the flows in the gas and heat networks are shown in Figs. 9 and 10, respectively.

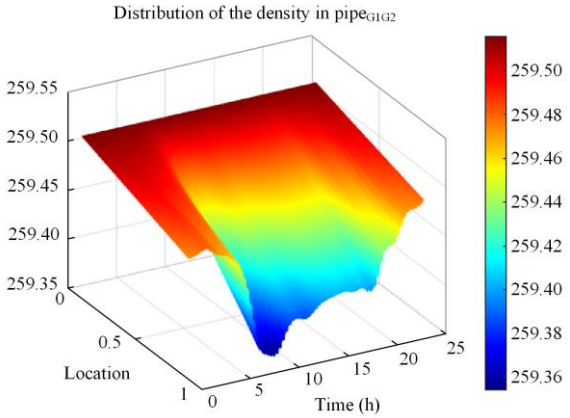

Fig. 9. Gas density distribution in one of the pipelines in the natural gas network.

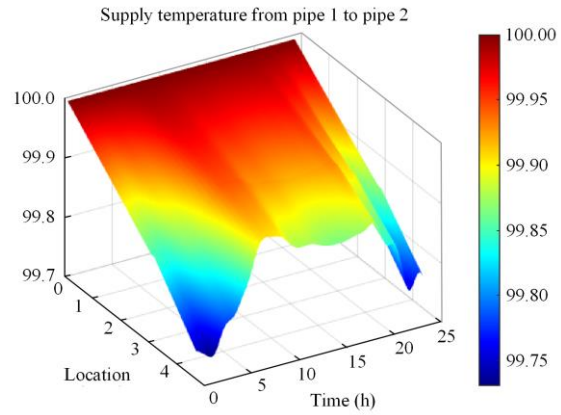

Fig. 10. Temperature distribution of one of the pipelines in the heat network.

B. Feasibility Analysis

To test the estimation accuracy, $S_{\mathrm{H}}/S_{\mathrm{M}}$, i.e., the ratio of the estimated error statistics S_{H} to the measurement error statistics S_{M}, is used to evaluate the filtering effect, and the lower the value, the better the filtering. S_{M} and S_{H} are given as:

$$S_{\mathrm{M}}=\frac{1}{T}\sum_{t=1}^{T}\left[\frac{1}{n}\sum_{n=1}^{n}\left[\frac{1}{m}\sum_{i=1}^{m}\left(\frac{z_i-h_i(x_{\mathrm{true}})}{\sigma_i}\right)^2\right]^{\frac{1}{2}}\right] \tag{48}$$

$$S_{\mathrm{H}}=\frac{1}{T}\sum_{t=1}^{T}\left[\frac{1}{n}\sum_{n=1}^{n}\left[\frac{1}{m}\sum_{i=1}^{m}\left(\frac{h_i(\hat{x})-h_i(x_{\mathrm{true}})}{\sigma_i}\right)^2\right]^{\frac{1}{2}}\right] \tag{49}$$

where T is the number of Monte Carlo simulations; n is the sampling times in a day; m is the number of measured values; x_{true} is the true value of the state variable; $\hat{x}$ is the estimated value; and σ_i is the standard deviation of superimposed noise.

Because of the random nature of a single experiment, 100 Monte Carlo simulation experiments are carried out, i.e., $T=100$. The multi-energy flow calculation result is regarded as the true value, and is added to a random variable with a Gaussian distribution. This is then used as the measurement of the IES.

When calculating the true value of multi-energy flow, to ensure accuracy, the difference step size of the gas and heat networks is set to 1 s. When state estimation is performed, the difference step size in the Kalman filter prediction step should be consistent with the sampling period, so the differential steps of the gas and heat networks are 120 s and 240 s, respectively. The energy flow results with different differential steps for the heat and gas networks are shown in Figs. 11 and 12, respectively.

It can be seen from Figs. 11 and 12 that, after adjusting the difference step sizes, the calculation results are not exactly the same as those before adjustment, but the change trend of state variables can still be tracked. Comparing the prediction results of the two networks, the prediction accuracy of the heat network is significantly higher than that of the gas network. This is because the model of the heat network is relatively simple, the mass flow rate in the same pipeline is equal everywhere, and its dynamic process is ignored. For the gas network, the mass flow rate and pressure in the pipeline are not equal everywhere but change all the time. Moreover, the state variables in the gas network show periodic oscillation and attenuation. This is because when the load is disturbed, not only the new load balance equations but also the dynamic equations must be satisfied, resulting in the persistence of gas inflation and deflation until the gas in the pipeline reaches a steady state. The pipelines in a gas network can be regarded as energy storage elements, similar to capacitors in electric power system. Therefore, the dynamic characteristics in the natural gas system are much more complicated than those in the thermal system.

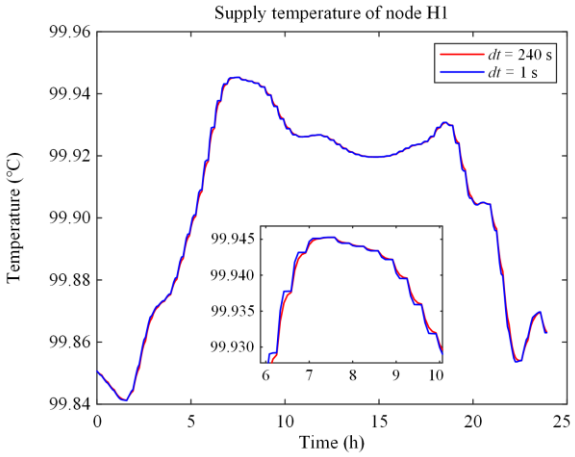

Fig. 11. Calculation results of energy flow with different differential steps in the heat network.

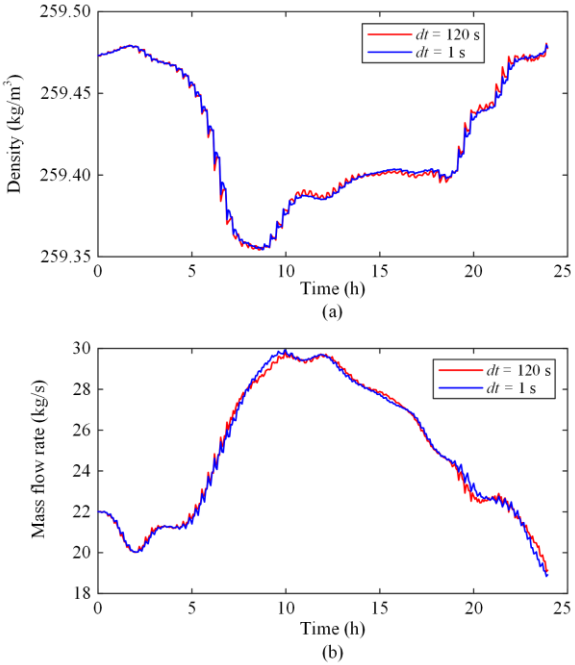

Fig. 12. Calculation results of energy flow with different differential steps in the gas network. (a) The density of node G2. (b) The mass flow rate of MF2.

To visually display the filtering effect in each network, the simulation results of some estimated values are shown in Figs. 13–15.

From Figs. 13–15, the following observations can be made:

1) In the electricity network, the voltage amplitude and phase angle change periodically. This is caused by the coupling of the electricity-gas-heat network. The load of the gas network is adjusted every 10 min, resulting in a

sudden change in the output of G1 every 10 min, while the load adjustment of the heat network will change the heat output of the CHP, thus changing the electric output.

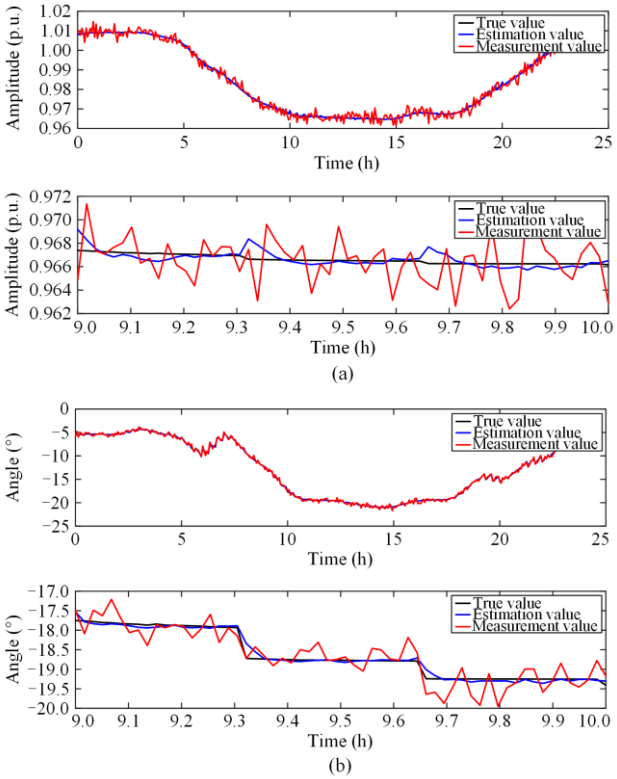

Fig. 13. State estimation results of node E4 in the electricity network. (a) Amplitude of node E4. (b) Angle of node E4.

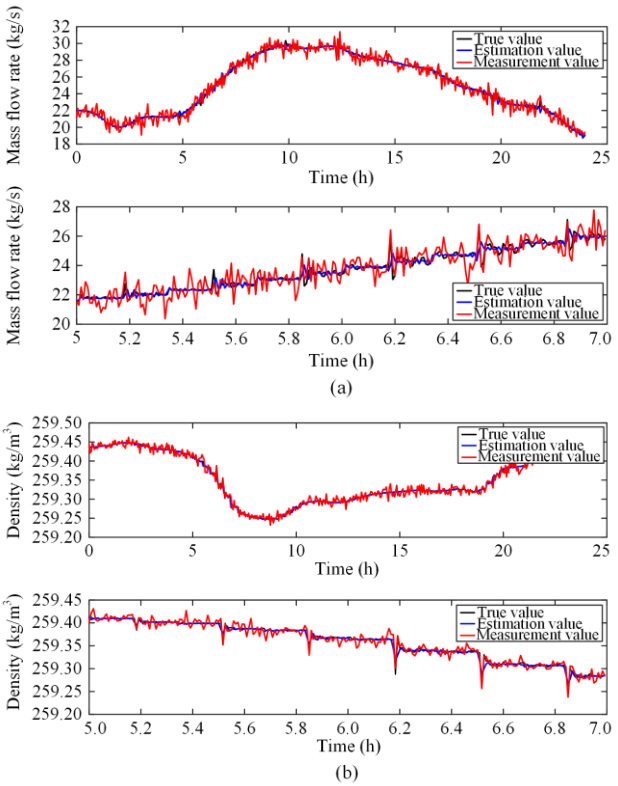

Fig. 14. State estimation results of node G3 and pipeline 2 in the gas network. (a) The mass flow rate of ME2. (b) The density of node G3.

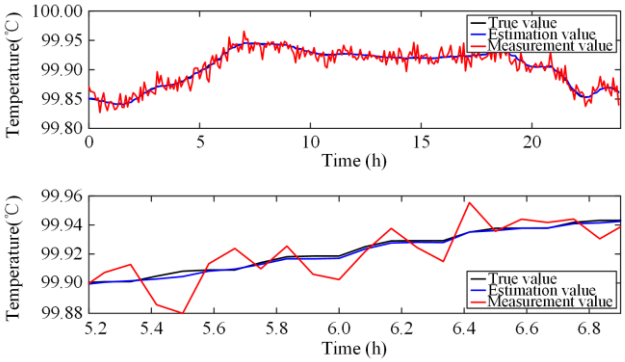

Fig. 15. State estimation results of node H3 in the heat network.

2) In the gas pipeline network, since the power and gas systems are unidirectionally coupled, the gas system acts as a constant output power source for the power system. Therefore, although the state variable of the gas network shows periodicity, it is only related to the load adjustments of the heat and natural gas networks.

3) Since the equivalent physical model of the heat network is simple, only the temperature needs to be estimated. It is not affected by the load changes of the electricity and gas networks, so the prediction is accurate and the filtered curve is smooth.

4) The natural gas and heat networks are represented by dynamic models, so even if their states change dramatically, the changing trends can still be tracked by the predicted steps, and after filtering the update steps, better estimation results can be obtained. In contrast, the electricity network has a quasi-steady state model. In the condition of a gentle load change, only the short-term state can be predicted by Holt's method in the prediction step, while the long-term change of the state cannot be tracked by the prediction alone. However, the measurement redundancy of the electricity network is much larger than those of the other networks, and good filtering results can also be corrected by measurement.

The quantitative indicators of the filtering results are shown in Table I. In Method 1, only the Kalman filter is used for state estimation, whereas in Method 2, the predicted values of the electricity and gas networks are adaptively adjusted according to (40) and (41). In method 3, based on method 2, adaptive robust weights are added according to (44) and (45).

TABLE I
FILTERING RESULTS WITHOUT BAD DATA

Network	S_H / S_M		
	Method 1	Method 2	Method 3
Electricity network	0.2667	0.2319	0.2404
Gas network	0.3094	0.2856	0.2866
Heat network	0.1732		0.1733

As shown in Table I, after the prediction is adaptively adjusted, the filtering accuracies in the power and gas networks have been improved, which shows that the method proposed in this paper is effective. The prediction

accuracy of the heat network is sufficiently high, and the filtering accuracy cannot be improved by adaptive adjustment, so Method 2 is not considered. For the gas and heat networks, there is almost no accuracy loss through the robust state estimation method (Method 3) without bad data, indicating that the proposed method is general for the gas and heat networks. Because of the large number of measurements in the electric power system and the strong nonlinear relationship with the state variables, the measurements with small errors may be misadjusted by the method in this paper, resulting in a decrease in the estimation accuracy. However, it is worthwhile to make the whole system robust by slightly reducing the filtering accuracy, as discussed below.

C. Feasibility Analysis

To ensure calculation efficiency, only a small number of samples are selected from the historical database as the kernel density estimation samples of the adaptive weights. It is assumed that 10 days are randomly selected from the historical 90 days, and a total of 10 samples are randomly selected from the time window of 1 hour before and after the current time, so 100 samples are required to calculate each measurement weight. Since measurements and samples are independent, weights for different measurements can be calculated simultaneously.

Only one bad data is set at the same time, and the calculation results are shown in Table II.

TABLE II
SETTING A SINGLE BAD DATA AT DIFFERENT TIME

Network	Bad data location	True value	Measurement	Estimated value
Electricity network	Branch active power (E1-E2)	1.9593	4.6829	1.9566
	Branch reactive power (E1-E2)	1.8296	7.6426	1.8296
	Node active power (E3)	−2.0815	3.46	-2.0811
	Node reactive power (E3)	−0.58	1.2	-0.5807
	Node voltage amplitude (E4)	0.9922	1.7828	0.9926
Gas network	Gas density (G3)	259.4407	210.1457	259.4425
	Mass flow rate (M_{E1})	28.4818	12.2241	28.4856
Heat network	Supply temperature (H3)	99.8683	49.7911	99.8680
	Return temperature (H3)	49.7911	99.8683	49.7902

It can be seen from Table II that a single bad data has almost no effect on the state estimation accuracy. The weight of the bad data is set to be close to zero so that it can be eliminated without using the bad data identification link. The determination of whether the measurement is bad data is done according to the weight value.

For multiple related bad data at the same time, the calculation results are shown in Table III. As seen, the estimation accuracy of the electricity network decreases when there are multiple related bad data at the same time. At this time, most of the measurements related to the node fail, but rough results can still be obtained by the forecasting-aided method, while the state estimation at the next moment will not be greatly affected. For the other two networks, because of the higher accuracy of the predicted values, the estimation accuracies are still high even if there are multiple correlated bad data at the same time. The above results show that the method proposed in this paper can overcome the influence of multiple types of bad data in each sub-network, and has good filtering results for normal measurement data.

TABLE III
SETTING MULTIPLE RELATED BAD DATA AT THE SAME TIME

Network	Bad data location	Time (min)	True value	Measur-e ment	Estimated value
Electricity network	Branch active power (E5-E6)	550	−5.4879	0	−5.5297
	Branch reactive power (E5-E6)		0.2655	−2.0365	0.2466
	Node active power (E5)		−5.0988	0.56	−5.1158
	Node reactive power (E5)		−0.56	−5.0988	−0.5927
	Node voltage amplitude (E5)		1.0068	0.6972	1.0062
Gas network	Gas density (G3)	720	259.2913	276.4562	259.2904
	Mass flow rate (M_{E1})		29.7026	15.0264	29.8075
Heat network	Supply temperature (H5)	800	99.7195	49.8805	99.7321
	Return temperature (H3)		99.8680	49.7964	99.8681

D. Influence of Different Measurement Periods on Estimation Accuracy

Without changing the adjustment time of the heat and gas networks, the measurement period is changed and its influence on the estimation accuracy is analyzed. The electric power system is in the quasi-steady state model, and changing the measurement period means that the time scale of the quasi-steady state changes. The final estimation results are shown in Table IV.

TABLE IV
SETTING MULTIPLE RELATED BAD DATA AT THE SAME TIME

Network	Measurement period					
	10 s	30 s	1 min	2 min	4 min	10 min
Electricity network	0.1404	0.1888	0.2180	0.2754	0.3474	0.5817
Gas network	0.2264	0.2499	0.2624	0.2851	0.3560	0.5497
Heat network	0.0975	0.1001	0.1104	0.1243	0.1726	0.4004

In the electricity network, the estimation accuracy increases with the shortening of the measurement period. This is because the change of state variables is small after the shortening of the measurement period, and there is rarely a large load fluctuation in a short period, so that the accuracy of the prediction step becomes higher, leading to high estimation accuracy.

For the gas network, the estimation accuracy is not significantly improved by reducing the measurement period from 2 min to 10 s. However, the estimation accuracy is decreased significantly by increasing the measurement period to 10 min. It shows that the prediction accuracy does not change much within these time scales (10–120 s). To reduce the calculation cost, it is reasonable to set the measurement period to 2 min. Moreover, a very long measurement period makes it difficult to capture the state dynamics, resulting in insufficient estimation accuracy.

Compared with the gas network, the dynamic characteristics of the heat network are slower and the model is simpler. A longer measurement period can be selected for a condition of sufficient accuracy, but the measurement period cannot be too long, for similar reasons to those for the gas network. When the measurement period is small, the uncertainty of the initial value makes the estimation accuracy of the heat network limited. Thus, reducing the measurement period cannot significantly improve the calculation accuracy, but will greatly increase the calculation cost. In the simulation calculation, the influence of uncertain factors such as the environment cannot be considered, the actual upper limit of accuracy will be lower, and it is uneconomical to set a shorter measurement period. Therefore, it is necessary to develop a multi-time-scale measurement strategy for the electricity-gas-heat coupled network.

VI. CONCLUSION AND FUTURE WORK

A. Conclusion

In this paper, based on a quasi-steady state model of the electric power system, dynamic models of the gas network and the heating system, combined with the Kalman filter framework and the kernel density estimation algorithm, a robust state estimation with multiple-time scale measurement for the electricity-gas-heat coupled network is proposed. The analysis shows that:

1) The dynamic models of the gas and heat networks based on the finite difference method provide accurate prediction values for the prediction step of state estimation. Reducing the measurement period can improve the accuracy of state prediction, but it will also increase the computational cost. Therefore, the measurement period should be adjusted according to the size of the system and the need for state estimation accuracy.

2) The adaptive measurement weight makes the IES state estimation robust, and different types of bad data can be identified through the method. It fits perfectly with the forecasting-aided state estimation used in this paper. Even if all measurements fail, rough results can still be obtained through state prediction. This reduces the impact of bad data on the current time section on future estimates.

B. Future Work

1) In terms of an IES model, the natural gas and heat networks are simplified in this paper, so more refined models can be considered in future work.

2) In terms of state estimation methods, the boundary conditions of the IES are not fully considered, so that some constraints cannot be fully satisfied, such as zero injection node constraints. Therefore, special treatment of boundary conditions and constraints should be considered in future work.

3) Although the coupling between the three networks is weak, intermittent disturbances still occur because of their different dynamic characteristics, especially the impact of load disturbances in the heat and gas networks on the electricity network. Therefore, in future work, the disturbance effect of the heat and the gas networks can be considered in the state prediction of the electricity network, and a deeper coupling relationship of the electricity-gas-heat network can be established.

ACKNOWLEDGMENT

Not applicable.

AUTHORS' CONTRIBUTIONS

Jianshu Yu: full-text writing and the construction of the paper framework. Dechang Yang: conceptualization, methodology. Jinye Cao: software and simulations. Payman Dehghanian: writing, reviewing, and editing. Nikita Tomin: technique guidance. All authors read and approved the final manuscript.

FUNDING

This work is supported by the National Natural Science Foundation of China (No. 51977212 and No. U2166208).

AVAILABILITY OF DATA AND MATERIALS

Not applicable.

DECLARATIONS

Competing interests: The authors declare that they have no known competing financial interests or personal relationships that could have appeared to influence the work reported in this article.

AUTHORS' INFORMATION

Jianshu Yu received the M.S. degree in electrical engineering from China Agricultural University, Beijing, China, in 2022. His research interest is state estimation in integrated energy system.

Dechang Yang received the M.S. degree in electrical engineering from China Agricultural University, Beijing, China, in 2008, and the Ph.D. degree in power system from TU Dortmund in 2012. He is currently an Associate Professor with the China Agricultural University and distinguished associate professor of Tibet Agriculture and Animal Husbandry University. His research interests are the active distribution network operation and control, integrated multi-energy system planning, economic dispatching, and optimal management.

Jinye Cao received the B.S. degree in Nanjing Tech University, in 2021. He is currently pursuing the M.S. Degree in electrical engineering from China Agricultural University. His research interest is virtual power plants and electricity markets.

Payman Dehghanian received the B.S. and M.S. degrees both in Electrical Engineering respectively from University of Tehran, Tehran, Iran, in 2009, and Sharif University of Technology, Tehran, Iran, in 2011. His research interests include power system reliability, reliability centered maintenance, and asset management.

Nikita Tomin received the Specialist degree in electrical engineering from Bratsk State University, Bratsk, in 2005, and the Ph.D. degree in electrical engineering from the Melentiev Energy Systems Institute, Siberian Branch of the Russian Academy of Sciences (RAS), Irkutsk,Russia, in 2007. His research interests include emergency management, learning (artificial intelligence), and power engineering computing.

REFERENCES

[1] D. Wang, L. Liu, and H. Jia *et al*., "Review of key problems related to integrated energy distribution systems," *CSEE Journal of Power and Energy Systems*, vol. 4, no. 2, pp. 130-145, Jun. 2018.

[2] B. Yun, E. ZHANG, and G. Zhang *et al*., "Optimal operation of an integrated energy system considering integrated demandresponse and a "dual carbon" mechanism," *Power System Protection and Control*, vol. 50, no. 22, pp. 11-19, Nov. 2022. (in Chinese)

[3] Y. Qiu, Q. Li, and Y. Ai *et al*., "Two-stage distributionally robust optimization-based coordinated scheduling of integrated energy system with electricity-hydrogen hybrid energy storage," *Protection and Control of Modern Power Systems*, vol. 8, no. 2, pp. 542-555, Apr. 2023.

[4] H. Sun, Z. Pan, and Q. Guo, "Energy management for multi-energy flow: challenge and prospects," *Automation of Electric Power Systems*, vol. 40, no. 15, pp. 1-8, Aug. 2016. (in Chinese)

[5] X. Hou, L. Ji, and S. Liu *et al*., "Self-healing and optimal operation strategy of the energy internet based on a bi-level optimization model,". *Power System Protection and Control*, vol. 50, no. 23, pp. 9-18, Dec. 2022. (in Chinese)

[6] H. Sun, Q. Guo, and W. Wu *et al.*, "Integrated energy management system with multi-energy flow for energy internet: design and application," *Automation of Electric Power Systems*, vol. 43, no. 12, pp. 122-128, Jun. 2019. (in Chinese)

[7] Q. Liu, H. Zhou, and Y. Zhang *et al*., "Security control strategy of an electricity-gas-thermal integrated energy system based on uniform power flow sensitivity,". *Power System Protection and Control*, vol. 49, no. 22, pp. 87-97, Nov. 2021. (in Chinese)

[8] Y. Wang, J. Gu, and L. Yuan, "Distribution network state estimation based on attention-enhanced recurrent neural network pseudo-measurement modeling," *Protection and Control of Modern Power Systems*, vol. 8, no. 2, pp. 508-523, Apr. 2023.

[9] J. Dong, H. Sun, Q. Guo *et al*., "State estimation for combined electricity and heat networks," *Power System Technology*, vol. 40, no. 6, pp. 1635-1641, Jun. 2016. (in Chinese)

[10] J. Dong, H. Sun, and Q. Guo *et al*., "State estimation of combined electric-gas networks for energy internet," *Power System Technology*, vol. 42, no. 2, pp. 400-408, Feb. 2018. (in Chinese)

[11] Y. Du, W. Zhang, and T. Zhang, "ADMM-based distributed state estimation for integrated energy system,". *CSEE Journal of Power and Energy Systems*, vol. 5, no. 2, pp. 275-283, Jun. 2019.

[12] S. Zheng, J. Liu, and Y. Chen *et al*., "Bilinear robust state estimation based on weighted least absolute value for integrated electricity-gas system," *Power System Technology*, vol. 43, no. 10, pp. 3733-3744, Oct. 2019. (in Chinese)

[13] Y. Chen, Y. Yao, and X. Yang *et al*., "Bilinear robust state estimation method for integrated electricity-heat energy systems," *Electric Power Automation Equipment*, vol. 39, no. 8, pp. 47-54, Aug. 2019. (in Chinese)

[14] Y. Chen, Y. Yao, and Y. Zhang, "A robust state estimation method based on SOCP for integrated electricity-heat system," *IEEE Transactions on Smart Grid,* vol. 12, no. 1, pp. 810-820, Jan. 2021.

[15] Q. Chen, D. Yang, and Y. Wang *et al*., "Robust state estimation of electricity-gas-heat integrated energy

system based on the bilinear transformations," *IET Generation Transmission & Distribution*, vol. 15, no. 1, pp. 149-163, Jan. 2021.

[16] J. Zhao, A. Gómez-Expósito, M. Netto *et al*., "Power system dynamic state estimation: motivations, definitions, methodologies, and future work," *IEEE Transactions on Power Systems*, vol. 34, no. 4, pp. 3188-3198, Jul. 2019.

[17] J. Yang, N. Zhang, and C. Kang *et al*., "Effect of natural gas flow dynamics in robust generation scheduling under wind uncertainty," *IEEE Transactions on Power Systems*, vol. 33, no. 2, pp. 2087-2097, Mar. 2018.

[18] J. Fang, Q. Zeng, and X. Ai *et al*., "Dynamic optimal energy flow in the integrated natural gas and electrical power systems," *IEEE Transactions on Sustainable Energy*, vol. 9, no. 1, pp. 188-198, Jan. 2018.

[19] K. Shu, X. Ai, and J. Fang *et al*., "Real-time subsidy based robust scheduling of the integrated power and gas system," *Applied Energy*, vol. 236, pp. 1158-1167, Feb. 2019.

[20] Y. Chen, Y. Yao, and Y. Lin *et al*., "Dynamic state estimation for integrated electricity-gas systems based on Kalman filter," *CSEE Journal of Power and Energy Systems*, vol. 8, no. 1, pp. 293-303, Jan. 2022.

[21] T. Zhang, W. Zhang, and Q. Zhao *et al.*, "Distributed real-time state estimation for combined heat and power systems," *Journal of Modern Power Systems and Clean Energy*, vol. 9, no. 2, pp. 316-327, Mar. 2021.

[22] H. Liu, C. Zhao, and S. GE *et al*., "Sequential power flow calculation of power-heat integrated energy system based on refined heat network model," *Automation of Electric Power Systems*, vol. 45, no. 4, pp. 63-72, Feb. 2021. (in Chinese)

[23] C. He, L. Wu, and T. Liu *et al*., "Robust co-optimization scheduling of electricity and natural gas systems via ADMM," *IEEE Transactions on Sustainable Energy*, vol. 8, no. 2, pp. 658-670, Apr. 2017.

[24] W. Wang, L. Yang, and L. Wang *et al*., "Optimal dispatch of integrated electricity-heat energy system considering heat storage characteristics of heating net work," *Automation of Electric Power Systems*, vol. 42, no. 21, pp. 45-52, Nov. 2018. (in Chinese)

[25] T. Sheng, G. Yin, and Q. Guo *et al*., "A hybrid state estimation approach for integrated heat and electricity networks considering time-scale characteristics," *Journal of Modern Power Systems and Clean Energy*, vol. 8, no. 4, pp. 636-645, Jul. 2020.

[26] J. Yang, N. Zhang, and A. Botterud *et al*., "Situation awareness of electricity-gas coupled systems with a multi-port equivalent gas network model," *Applied Energy*, vol. 258, Nov. 2020.

[27] B. Chen, H. Sun, and Y. Chen *et al*., "Energy circuit theory of integrated energy system analysis (I): gaseous circuit," *Proceedings of the CSEE*, vol. 40, no. 2, pp. 436-444, Jan. 2020. (in Chinese)

[28] J, Yang, N. Zhang, and A. Botterud *et al.*, "On an equivalent representation of the dynamics in district heating networks for combined electricity-heat operation," *IEEE Transactions on Power Systems*, vol. 35, no. 1, pp. 560-570, Jan. 2020.

[29] B. Chen, H. Sun, and G. Yin *et al*., "Energy circuit theory of integrated energy system analysis (II): energy circuit theory of integrated energy system analysis (II): hydraulic circuit and thermal circuit," *Proceedings of the CSEE*, vol. 40, no. 7, pp. 2133-2142, Apr. 2020. (in Chinese)

[30] J. Yu, D. Yang, and Z. Chen, "Multi-energy flow calculation based on energy cell and parallel distributed computation," *International Journal of Electrical Power & Energy Systems*, vol. 131, 2021.

[31] X. Liu, J. Wu, and N. Jenkins *et al*., "Combined analysis of electricity and heat networks," *Applied Energy*, vol. 162, pp. 1238-1250, Jan. 2016,.

[32] J. Zhao, G. Zhang, and M. La Scala, "PMU based robust dynamic state estimation method for power systems," in *2015 IEEE Power & Energy Society General Meeting*, Denver, USA, Jul. 2015, pp. 1-5.